J Mater Sci (2015) 50:5993–6006
DOI 10.1007/s10853-015-9147-1

Optimization of the CaO and P_2O_5 contents on PDMS–SiO_2–CaO–P_2O_5 hybrids intended for bone regeneration

D. A. Sánchez-Téllez[1] · L. Téllez-Jurado[1] · L. M. Rodríguez-Lorenzo[2,3]

Received: 7 April 2015 / Accepted: 2 June 2015 / Published online: 9 June 2015

Abstract Osteoproductive materials that induce quick bone regeneration are needed for the developing area of scaffold-based bone engineering. Bioactive silica-based glasses, ceramics, and hybrids are called to play an important role in this field. Organic–inorganic hybrid materials based on SiO_2-modified PDMS–P_2O_5–CaO are studied in this work. These materials are synthesized by the sol–gel method, and the influence of the composition on the reaction kinetic, obtained porosities, degradation and bioactive behavior, and cytotoxicity is studied. Materials with greater contents in CaO yield faster reaction kinetics and produce porous materials that favor a quicker degradation, whereas with greater P_2O_5 contents produce denser and more stable materials. The incorporation of CaO and P_2O_5 up to 5 and 25 % in weight into the SiO_2 network, respectively, resulted in an increase of the apatite-forming ability in PBS. None of the studied compositions are cytotoxic, showing cellular viability over 70 % at all times.

✉ D. A. Sánchez-Téllez
danielatellez06@gmail.com

[1] Depto. de Ing. en Metalurgia y Materiales, Instituto Politécnico Nacional-ESIQIE, UPALM-Zacatenco, 07738 Mexico, D.F., Mexico

[2] Biomaterials Group, ICTP-CSIC, Juan de la Cierva, 3, 28006 Madrid, Spain

[3] Networking Biomedical Research Centre in Bioengineering, Biomaterials and Nanomedicine (CIBER-BBN), Madrid, Spain

Introduction

Consolidation delays are one of the main causes of clinical complications on repairing bone fractures. This is particularly important for the repair of low-quality bone fractures such as osteoporotic bone fractures or in critical size defects [1]. A promising approach to prevent these complications is to prepare the fixation device with osteoproductive materials that induce quick bone regeneration. Ideally, these materials should be slowly degrading materials that at the same time sustain sufficient strength to ensure their structural stability until the completion of a functional tissue formation [2]. However, currently applied scaffold designs use fast-degrading polymers, which, in combination with high-porosity (90 %) matrixes, do not provide an appropriate degradation rate and the required structural stability to resist the physiological loads that occur during the processes of integration and healing.

Bioactive ceramics [3, 4] and bioactive glasses [5–7] have been investigated for bone repair and regeneration due to their attractive properties, such as good biocompatibility and good osseointegration when bonding spontaneously to living bone tissue; however, their clinical application is limited due to their fragility, low mechanical resistance to impact, and tensile and bending forces.

The sol–gel process has been studied in the field of bioceramics and bioglasses. The combination of silica-based glasses with organic compounds, chemically incorporated into the molecular structure of the vitreous silica, yields organic–inorganic hybrid materials [5]. The porosity and the bioactive behavior of these hybrids can be controlled to a nanometer scale. Furthermore, the biocompatibility, thermal, mechanical, degradative, and bioactive properties of these hybrid materials may be tailored with the sol–gel synthesis to the desired target. Bioactivity is

Table 1 Sample codes, molar and weight ratios, gelling times, and bulk densities of the hybrids

Sample	Molar ratio			Weight ratio			Gelling time (h)	Density, ρ (g/cm^3)
	TEOS = 1							
	H_2O	HCl	i − Pr	PDMS + TEOS = 1	Ca/TEOS = 1	P_2O_5/TEOS = 1		
Ca0P5	3	0.3	4.5	0.3 + 0.7 = 1	0	5	1.15	1.0 ± 0.1
Ca5P5					5	5	0.20	1.03 ± 0.02
Ca5P15					5	15	1.33	1.06 ± 0.09
Ca5P25					5	25	39.5	0.87 ± 0.02
Ca5P50					5	50	98.28	1.1 ± 0.07
Ca5P75					5	75	101	1.335 ± 0.005
Ca40P1					40	1	0.50	0.805 ± 0.005
Ca40P3					40	3	0.41	0.805 ± 0.005

one of the required properties for materials designed for bone regeneration. Bioactivity is related with the ability of growing an apatite layer on the surface of the material [5–7], and it has been concluded that the formation and growth of this layer is favored by the release of calcium ions and the formation of silanol groups on the materials' surfaces. Hesaraki et al. [8] synthesized bioactive silico-phosphate glasses with calcium and calcium/strontium. It was observed that calcium favored precipitation of a calcium phosphate layer on the materials' surface when immersed in SBF and the proliferation of osteoblastic rat cells. On the other hand, Lee et al. [9] used tetraethoxysilane (TEOS) as a bioactive silica precursor to hybridize the surface of polydimethylsiloxane (PDMS) by the sol–gel method. The hybrid showed a SiO_2–PDMS cross-linked structure, providing this material with the bioactive behavior of the ceramic (TEOS–SiO_2) and the physical properties of the polymer (PDMS–OH–$[Si(CH_3)_2–O]_nH$). However, the influence of the composition on the structure, physical properties, and, as a consequence, on the bioactivity and cellular interaction of this family of hybrids has not been studied in detail. The purpose of this work is to develop an SiO_2-based bioactive hybrid material and to study the influence of the composition on the structure, degradation kinetics, bioactivity, and cytotoxicity of the material.

Experimental procedure

Synthesis of the hybrid materials

Hybrid materials were synthesized using the sol–gel method. The starting reagents were hydroxyl-terminated polydimethylsiloxane (PDMS, OH–$[Si(CH_3)_2–O]_nH$, Aldrich, MW = 550 gmol, viscosity = 25 cSk), (TEOS, $Si(OCH_2CH_3)_4$, Aldrich), triethyl phosphate (TEP, $C_6H_{15}O_4P$, Sigma-Aldrich), calcium nitrate tetrahydrate ($Ca(NO_3)_2·4H_2O$, Fermont), isopropanol (IPA, Aldrich), deionized water, and hydrochloric acid (HCl 37 %, Fermont) as a catalyst. Molar and weight ratios of the starting solutions used during the synthesis are listed in Table 1 together with the sample codes of the obtained compositions. The sample codes are assigned according to the weight percentage of calcium and phosphate in each hybrid material, e.g., Ca0P5 stands for 0 % in weight of Ca and 5 % in weight of P_2O_5. The synthesis process for hybrids starts with the preparation of four solutions [10], each one of them containing the same amount of IPA. The first solution contains TEOS and PDMS. The second solution contains water and HCl. The third solution contains TEP, and the fourth solution contains the CaO precursor and water. All solutions are stirred for 30 min at room temperature for homogenization. Then, the first and the second solutions are mixed in a boiling flask at 80 °C under refluxing and stirring. The TEP and CaO solutions were added drop wise for every 30 min. When the addition has finished, the sols were poured into a plastic container and kept at room temperature for gelling and aging. The products were dried at 100 °C for 24 h and named as hybrid materials. Finally, after drying, the hybrids were heat treated at different temperatures, up to 800 °C.

Characterization of the hybrid materials

The dried materials were characterized by Fourier transform infrared spectroscopy (FT-IR) in a Perkin Elmer Spectrum GX 74904, studying the region 4000–600 cm^{-1} with a resolution of 2 cm^{-1} and 16 scans performed per sample. X-ray diffraction (XRD) patterns were taken in a D8 FOCUS BRUKER diffractometer using Cu Kα radiation in the range of 10°–80° 2θ with a step size of 0.02° and a time per step of 0.5°/min. Magic angle spinning-nuclear

magnetic resonance (MAS-NMR) spectra were taken in a Bruker Avance TM 400WB spectrometer equipped with a superconducting magnet wide mouth (89 mm) operating at 9.4 Tesla with a frequency of 400 MHz. Thermal gravimetric analysis (TGA) was performed on a TA INSTRUMENTS TGAQ500 using a dynamic atmosphere of nitrogen at a flow rate of 100 mL/min and a heating rate of 10 °C/min. Scanning electron microscopy (SEM) was performed using a JEOL 3600 CFX Microscope with a voltage of 5 kV. The bulk density of the hybrid materials was evaluated using the Archimedes principle in a Sartorius AG Germany ME254S balance. Four specimens of each composition were immersed in ethanol, yielding an average density. Ethanol was chosen as a pushing liquid.

In vitro assays, degradability, bioactivity, and cytotoxicity

The hydrolytic degradation and bioactivity of the hybrid materials, dried at 100 °C, were tested by soaking specimens into 25 mL of phosphate buffer solution (PBS) at 36.5 °C and a pH of 7.4. Four replica of each hybrid material were used. The samples were soaked at the intervals of 1, 3, 7, 14, 21, and 28 days and weighed after drying at 36 °C. The remaining weight was calculated as weight remaining $(\%) = \frac{w2}{w1} \times 100$, where $w1$ and $w2$ are the weights of the samples before and after degradation, respectively. pH measurements of the soaking fluids were taken with a LAB pH METER PHM220 from MeterLab®. After drying, the specimens were analyzed by FT-IR, XRD, and SEM.

Cytotoxicity assays were carried out using osteosarcoma-like cells and the MTT assay. The cells were cultured in a semi-complete medium [Dulbecco's Modified Eagle Medium, Sigma (DMEM)], which was supplemented with 200 mM L-glutamine and 50 mg/mL gentamicin for 500 mL of medium. The culturing of the cells was carried out at 37 °C in a humidified atmosphere of 95 % air and 5 % CO_2 (standard conditions). The specimens were sterilized with UV light for 24 h, soaked into 5 mL of fresh sterile medium in plastic bottles, and placed in an incubator with constant stirring at 37 °C. Once the materials have been immersed for 1, 2, 7, 14, and 21 days, the "old medium" was removed and frozen. The cells were seeded in 100 μL of that "old medium" into 96-well culture plates at a density of 5×10^4 cells/mL per well. The reduction of the MTT reagent (3-[4,5-dimethylthiazol-2-yl]-2,5-diphenyltetrazolium bromide) was taken as an indicator of the cell viability of the materials. The data are presented as mean ± standard deviation (SD) of three independent experiments. The differences between the different compositions were evaluated by the analysis of variance statistical method (one-way ANOVA). Differences were considered statistically significant for $p < 0.05$.

Results

Synthesis of the hybrid materials

The hydrolysis–condensation reactions [11] involved in the sol–gel process are shown in Fig. 1. The SiO_2 precursor (TEOS) and the P_2O_5 precursor (TEP) are hydrolyzed to form silanol (Si–OH) and phosphanol (P–OH) groups, respectively. Once the hydrolysis is completed, the silanol and the phosphanol groups condense forming a continuous inorganic matrix made of SiO_2 and $O{=}P(O^-)_3$. The organic modification of the SiO_2–P_2O_5 network is done through the incorporation of poly(dimethylsiloxane) (PDMS), an organic modifier and network extender. The hydroxyl groups (–OH) at the end of the PDMS polymeric chains condense with some of the silanol and phosphanol groups, extending the SiO_2 network and giving to the material some of the PDMS properties. The molar and weight ratios of calcium and phosphate used to synthesize the materials, the sample codes, the resulting gelling times, and the densities are presented in Table 1. Comparing the gelling time of Ca0P5 with that of Ca5P5, a shorter gelling time can be observed when calcium is incorporated into the reaction for same P content. These results suggest that, with the addition of CaO, the resulting SiO_2–P_2O_5 chains are shorter, which results in an increase in the rate of condensation reactions and a reduction in the gelling time. The influence of the phosphate content on the gelling time for materials with the same CaO content can be better appreciated in Fig. 2. In this figure, it can be observed that gelling time increases significantly with the phosphate content, for phosphate contents between 15 and 50 wt%. These results indicate that phosphanol groups act as a network former and the greater content of phosphate slows down the condensation of the silanol and phosphanol groups yielding greater gelling times.

Hybrids' characterization

The FT-IR spectra of the synthesized hybrid materials are shown in Fig. 3a. In each of the spectra, the main characteristic absorption bands of the SiO_2–P_2O_5 glasses appear between 2000 and 600 cm^{-1} [12]. The band located at 800 cm^{-1} is assigned to Si–X bonds, where X = O, C; Si–O bonds correspond to the silicon tetrahedrons [SiO_4] and Si–C bonds belong to the PDMS [13]. The band at 848 cm^{-1} corresponds to the bonds between Q units (SiO_2) and D units (PDMS) in the cross-linked structure of the hybrid materials; in other words, it is assigned to (PDMS)

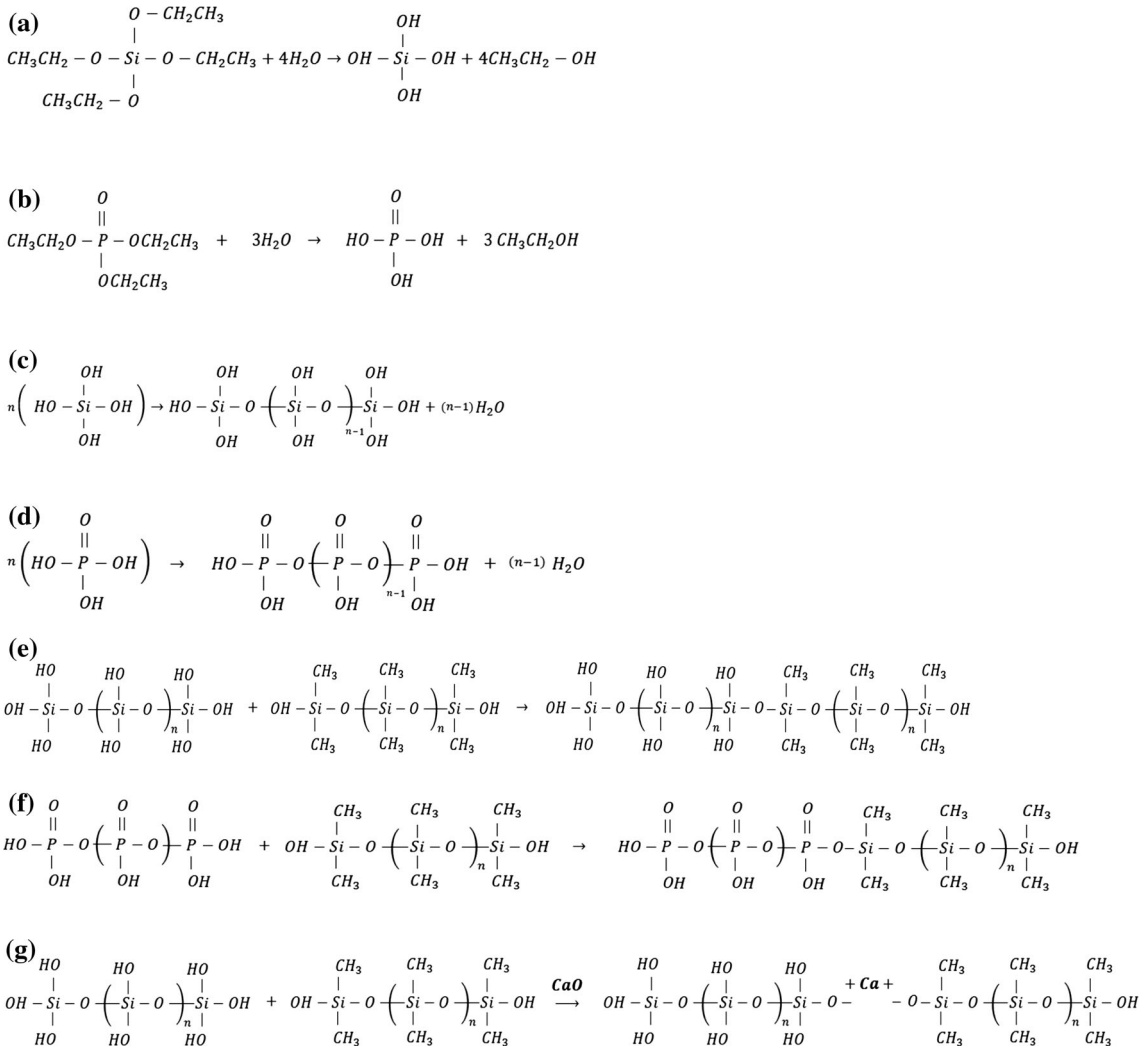

Fig. 1 **a** Hydrolysis reactions of SiO_2 precursor. **b** Hydrolysis reactions of P_2O_5 precursor. **c** Condensation reactions between silanol groups. **d** Condensation reactions between phosphanol groups. **e** Polycondensation reactions between silanol groups and PDMS. **f** Polycondensation reactions between phosphanol groups and PDMS. **g** CaO as an SiO_2–P_2O_5 network modifier

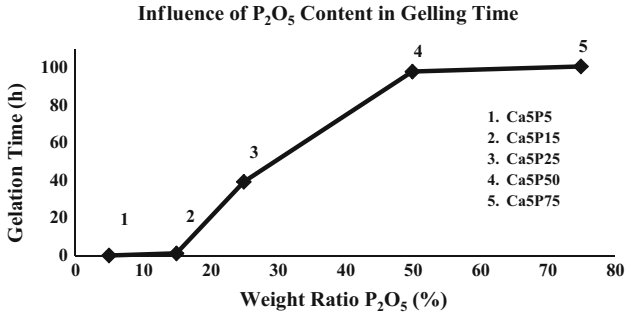

Fig. 2 Influence of P_2O_5 content in hybrid materials during gelling time

Si–O–Si (TEOS) bonds [14, 15]. The band located at 1262 cm^{-1} is related to the asymmetric stretching vibration of the Si–CH_3 bonds from the PDMS [16–18]. The bands located at 1030 and 1070 cm^{-1} are attributed to the Si–O–Si and PO_4 groups, respectively, both with stretching vibrations, and are related to the silica (SiO_2) and phosphate (P_2O_5) structure [12, 19]. The band at 1100 cm^{-1} is attributed to the P–O bonds related to P–O–P and P–O–Si units [12]. This band is also attributable to the asymmetric stretching mode from Si–O–Si bonds [13, 20]. The band observed at 958 cm^{-1} is assigned to the stretching vibration of the Si–OH and P–OH bonds, which are related to the hydrolyzed silanol and phosphanol groups, respectively [19, 21]. It is important to stand out that, whereas phosphanol containing materials display P–OH bands at 954 and 3676 cm^{-1}, silica-containing materials display Si–OH bands at 970 and 3750 cm^{-1} [21]. On the other hand, this band can also be related to the broken Si–O non-bridging bonds, which are commonly observed in SiO_2 glasses and gels [14]. Some bands assigned to nitrate groups, which are

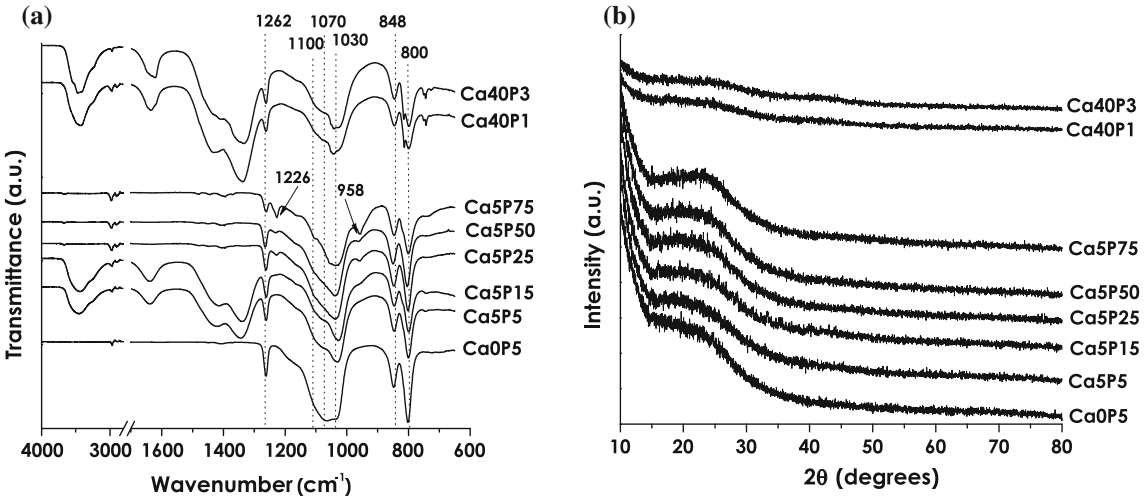

Fig. 3 **a** FT-IR spectra of the hybrid materials. **b** XRD patterns of the hybrid materials

attributed to the remaining precursor of calcium, $Ca(NO_3)_2 \cdot 4H_2O$, are located at 1419, 1339, 1044, and 745 cm^{-1}. As the phosphate content increases, the broad band located between 1100 and 1030 cm^{-1} shifts toward $\sim$1040 cm^{-1}, suggesting a greater amount of tetrahedral phosphate [PO_4] content. Furthermore, a band at 1220 cm^{-1} appears in the hybrids with higher phosphate content and it can be attributed to the vibration of the P=O bonds in the stretching mode of the metaphosphate groups $(PO_3)^{-1}$ [12]. On the other hand, the broad band observed at $\sim$3400 cm^{-1}, with a small shoulder at $\sim$3300 cm^{-1}, appears only for the Ca5P5, Ca5P15, Ca40P1, and Ca40P3 materials, and it is attributed to the –OH groups with an elongation and bending vibration associated to the Si–OH and P–OH groups and the adsorbed moisture from the environment [12, 14, 17, 19]. Another band that appears only in these four hybrids is the one at 1640 cm^{-1} assigned to the deformation of molecular water adsorbed [12, 14]. These two bands are present in the four hybrids mentioned above due to the amount of $Ca(NO_3)_2 \cdot 4H_2O$ added to the SiO_2 matrix in relation to the amount of phosphate content. While in these materials the water molecules and nitrates are trapped within the vitreous silica network, the tetrahedral SiO_2 and P_2O_5 in the materials with greater phosphate content do not bond completely due to the chemically neutral oxygen in P_2O_5, causing a less-interconnected silico-phosphate network and therefore allowing the water molecules and nitrates being released during syneresis and aging processes.

The XRD patterns of the hybrid materials are shown in Fig. 3b. A characteristic maximum of silica gels around 2θ 10°–14° can be observed in all samples, which may be attributed to aggregates of discrete particles with sizes between 10 and 100 Å [22]. This maximum is less pronounced for greater phosphate contents. Also, the materials exhibit a maximum at around 2θ 22.5°, which is stronger for greater phosphate contents. This maximum is typical in the XRD patterns of vitreous silica, and it is attributed to materials having short-range order [22].

^{29}Si and ^{31}P MAS-NMR spectra of the Ca0P5 hybrid dried at 100 °C are shown in Fig. 4. The ^{29}Si MAS-NMR spectra illustrate a symmetric peak with a chemical shift of −19 ppm, which corresponds to structural units (D) of dimethylsiloxane [$(CH_3)_2 \cdot SiO_2$]. Another peak is observed with a chemical shift of $\sim$−110 ppm. These shift values correspond to Q_3 and Q_4 structural units [14, 23, 24]. They can be attributed to the coordination of $Si(OSi)_3(OH)$ Q_3 or $Si(OSi)(OH)_2(OP)$ and $Si(OSi)_4$ Q_4 or $Si(OSi)_2(OP)(OH)$ [19]. On the other hand, the ^{31}P MAS-NMR spectra illustrate a wide band with a chemical shift of 0 which may correspond to Q_0 and −30 ppm which may correspond to Q_1 and Q_2 [25, 26]. Regarding the resonance around 0 ppm, it can be attributed to the chemical species with a high degree of shifting, such as phosphate-isolated units, assigned to the Q_0 units [25], corresponding to $O=P(OH)_3$ [19]. Thus, it can be said that the structure of the Ca0P5 hybrid material is formed by tetrafunctional Q_n chains with $[SiO_4]^{4-}$ ($n = 3, 4$) and $[PO_4]^{3-}$ ($n = 0, 1, 2$) structural units and difunctional units D_n ($n = 1,2$) [$(CH_3)_2 \cdots SiO_2$]. According to the previous results, it can be said that the silanol groups of the PDMS chains and $[PO_4]^{3-}$ groups are cross-linked with the SiO_2 network of the material Ca0P5 during the polycondensation reactions.

To study the thermal stability and to establish the average temperature at which PDMS decomposes in the presence of calcium and phosphate, the hybrid materials were heat treated up to 800 °C. The TGA results for representative hybrids dried at 100 °C are shown in Fig. 5. The thermogravimetric profile curves of the hybrid materials illustrate different behaviors among them. The TGA curve of the sample Ca0P5 exhibits a total weight loss of

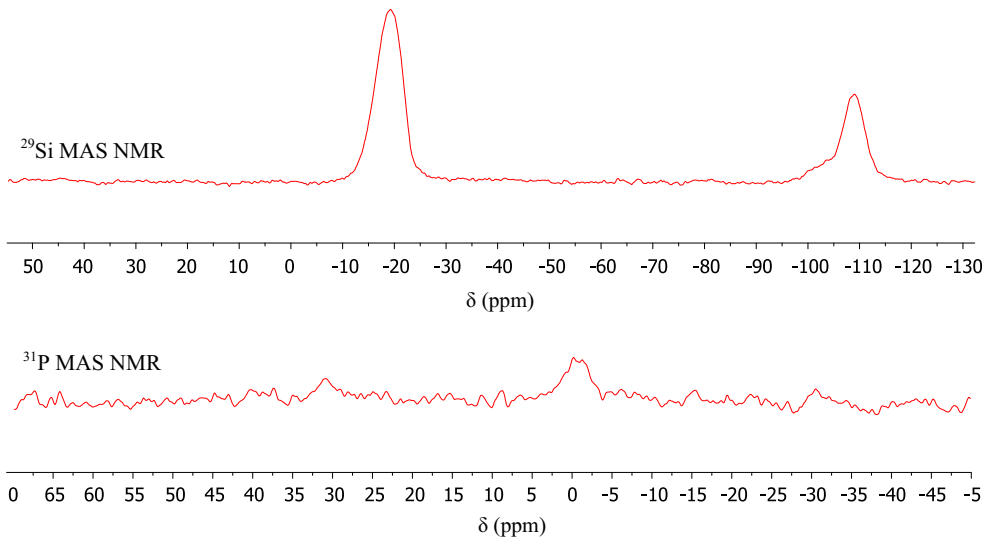

Fig. 4 ^{29}Si and ^{31}P MAS-NMR spectra of the Ca0P5 hybrid material

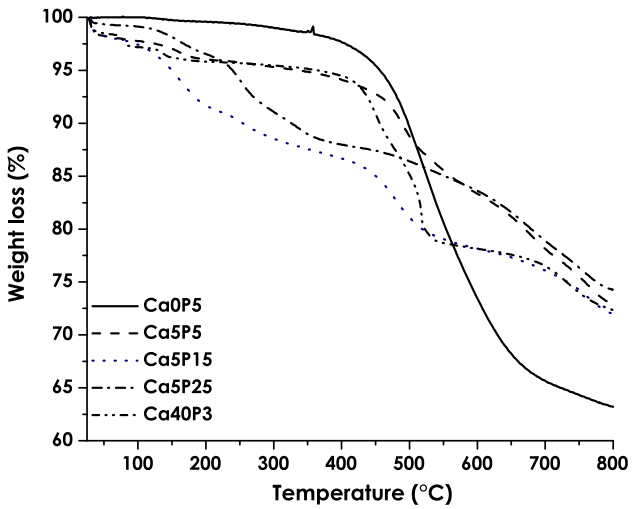

Fig. 5 TGA curves of representative hybrid materials

about 38 % up to 800 °C. The small weight loss observed at low temperatures can be attributed to the low hygroscopicity of the material [27]. The main weight loss occurs between 450 and 650 °C. This step can be related to the break of the cyclic oligomers, which has been described to occur at above 400 °C [14, 25, 28]. Another step occurs at above 650 °C which may be attributed to allotropic changes inside the material network [27].

The total weight losses of materials, Ca5P5, Ca5P15, and Ca5P25, are about 27, 27, and 25 %, respectively. These materials show a weight loss throughout the thermal range analyzed and fail to achieve thermal stability up to 800 °C. Different weight loss steps that can be related to their chemical composition are observed. Weight losses below 100 °C are attributed to the desorption of adsorbed water on the materials' surfaces. The weight loss percentage increases in this temperature range for greater calcium contents. This can be attributed to the addition of $Ca(NO_3)_2{\cdot}4H_2O$ as a calcium precursor that increases the hygroscopicity of the materials [27]. This effect is mainly seen in the Ca5P5, Ca5P15, Ca40P1 (data not shown), and Ca40P3 materials. The next weight loss step occurs at around 150 °C, which is associated to the loss of residual water and ethanol trapped within the materials' networks due to the continuous hydrolysis–condensation reactions [13, 14, 25, 28]. The third weight loss is observed between 190 and 270 °C, for the materials with higher phosphate content (Ca5P15, Ca5P25, Ca5P50, and Ca5P75). This weight loss is related to the decomposition of inorganic phosphate (HPO_4^{2-}) into pyrophosphate groups and water ($P_2O_7^{4-} + H_2O$) [27]. The fourth weight loss occurs at a temperature range between 350 and 430 °C, at which PDMS decomposition starts to form cyclic oligomers. Depending on the material, above 400 °C the final decomposition of PDMS oligomers occurs [14, 25, 28]. For the materials in which calcium has a great influence on their structures (Ca5P5, Ca5P15, Ca40P1, and Ca40P3), there can be observed the thermal decomposition of nitrate groups at a temperature range between 490 and 530 °C [14, 25, 27, 28]. Also, for those materials, the calcite ($CaCO_3$) starts to crystallize at around 500 °C and its decomposition into CaO and CO_2 occurs between 620 and 850 °C [27]. Finally, for materials with greater amount of phosphate, weight losses above 700 °C are associated to allotropic changes [27], such as the formation of several crystal phases.

The FT-IR spectra of the hybrid materials Ca0P5 and Ca5P5 thermally treated at different temperatures are shown in Fig. 6 as an example of the evolution of the spectra of the

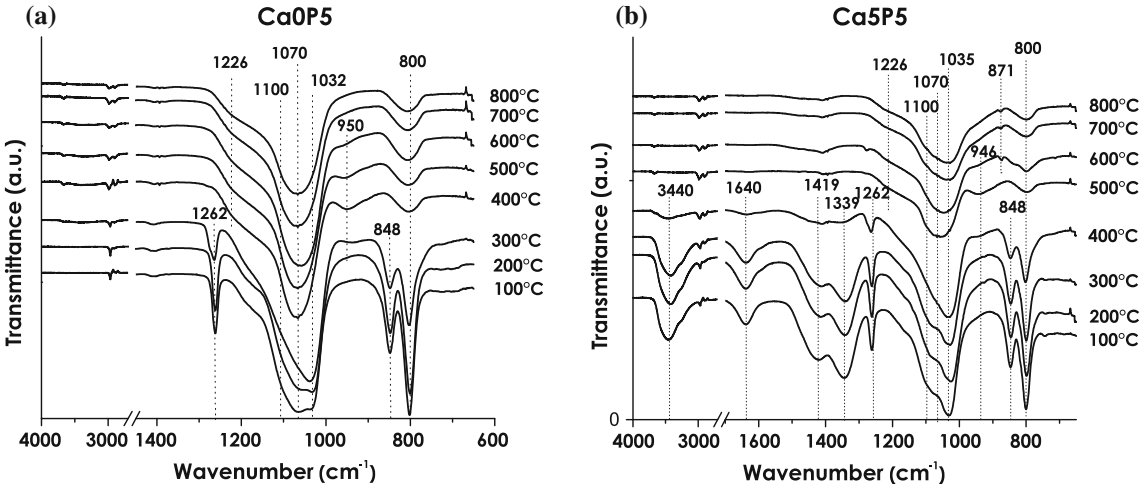

Fig. 6 FT-IR spectra of **a** the Ca0P5 and **b** the Ca5P5 hybrid materials thermally treated at different temperatures

hybrids with temperature. In these spectra, the transformation process of the hybrids into phospho-silicate glasses can be seen. Spectra of the material Ca0P5 (Fig. 6a) at 100 and 200 °C do not show significant changes between them. At 300 °C, the bands assigned to PDMS at 800, 848, and 1262 cm^{-1} decrease in intensity, corresponding to the initial degradation of PDMS and the beginning of the transition of the material from hybrid to glass. Similarly, the wide band in which the bands at 1100, 1070, and 1032 cm^{-1} are overlapped and assigned to the bonds Si–O–Si/P–O–P/P–O–Si, PO_4, and Si–O–Si, respectively, changes in shape and shifts slightly toward 1040 cm^{-1}. When increasing the temperature up to 400 and 500 °C, the spectra show great changes and PDMS-associated bands disappear (1262 and 848 cm^{-1}) or decrease in intensity (800 cm^{-1}), indicating that tetrahedral [SiO_4] are rebonded to form a more orderly network and thus the transformation of the hybrid material into a silico-phosphate glass. Moreover, bands located at 950 and ~1220 cm^{-1} appear and they can be related to hydrolyzed tetrahedral Si–OH groups [21] and P=O bonds in metaphosphate chains, respectively [12]. Furthermore, the overlapped bands between 1100 and 1030 cm^{-1} shift toward ~1080 cm^{-1}, which suggests a greater contribution of [PO_4] groups and the appearance of Si–O–P bonds [19]. Spectra registered at 600, 700, and 800 °C treatments are very similar to each other. The bands located at 800, 1080, and 1220 cm^{-1} remain without changes in comparison with the same bands in the spectra described before. However, the band at 950 cm^{-1} disappears at 700 °C, meaning a reduction or disappearance of the phosphanol (P–OH) groups due to condensation reactions to form linear chains and a cross-linked network along with SiO_2 in a continuous silico-phosphate inorganic matrix. The spectra of the material Ca5P5 treated at different temperatures are displayed in Fig. 6b. Bands assigned to nitrate groups at 1419, 1339, 1044, and 745 cm^{-1} together with the bands assigned to –OH groups from water and Si–OH and P–OH hydrolyzed groups at 3440 and 1640 cm^{-1}, appear in the spectra of this hybrid in contrast to the data obtained for the Ca0P5 hybrid. The bands associated to Si–CH_3 bonds and –OH groups decrease in intensity as the temperature increases . At 500 °C, those bands completely disappear. At 400 °C, a shoulder that is related to the vibration mode of Si–O–Ca [20] arises at 946 cm^{-1}. At 600 °C, a small band at 871 cm^{-1} attributed to carbonate groups CO_3^{2-} [29], associated to crystalline calcite, appears. The broad band located between 1035 and 1100 cm^{-1} increases in intensity when increasing the phosphate content due to the formation of a 3-D network of SiO_2–P_2O_5 with P–O–P and P–O–Si bonds.

The XRD patterns of the hybrid materials Ca0P5 and Ca5P5 thermally treated at different temperatures are shown in Fig. 7. The XRD patterns of the material Ca0P5 at 100, 200, and 300 °C are very similar to one another, no major changes are observed, neither do diffraction peaks appear, and therefore the material maintains the amorphous character. After the thermal treatment at 400 °C, the maximum associated to vitreous SiO_2 gets stronger and shifts toward 22.8° in 2θ, suggesting the transformation of the material from a hybrid to a silico-phosphate glass. At 800 °C, this maximum keeps shifting toward ~21.5° and increasing in intensity. On the other hand, the material Ca5P5 keeps its amorphous character up to 400 °C. When Ca5P5 is treated at 500 °C, calcite ($CaCO_3$) crystallizes within a glassy matrix and the characteristic maximum of the amorphous material decreases, suggesting the formation of a glass-ceramic material. The crystallization of other silico-phosphate phases seems to be inhibited. At 800 °C, most of the peaks attributed to calcite ($CaCO_3$) have disappeared.

The bulk densities of the materials are presented in Table 1. These bulk densities reflect a behavior that is consistent with the chemical composition and physical

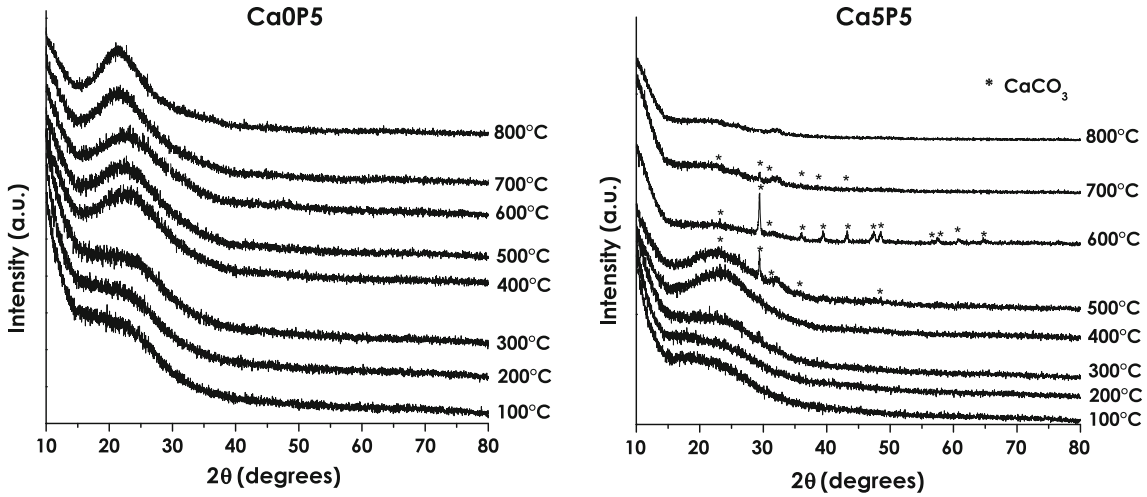

Fig. 7 XRD patterns of the Ca0P5 and Ca5P5 hybrid materials dried in air and thermally treated at different temperatures

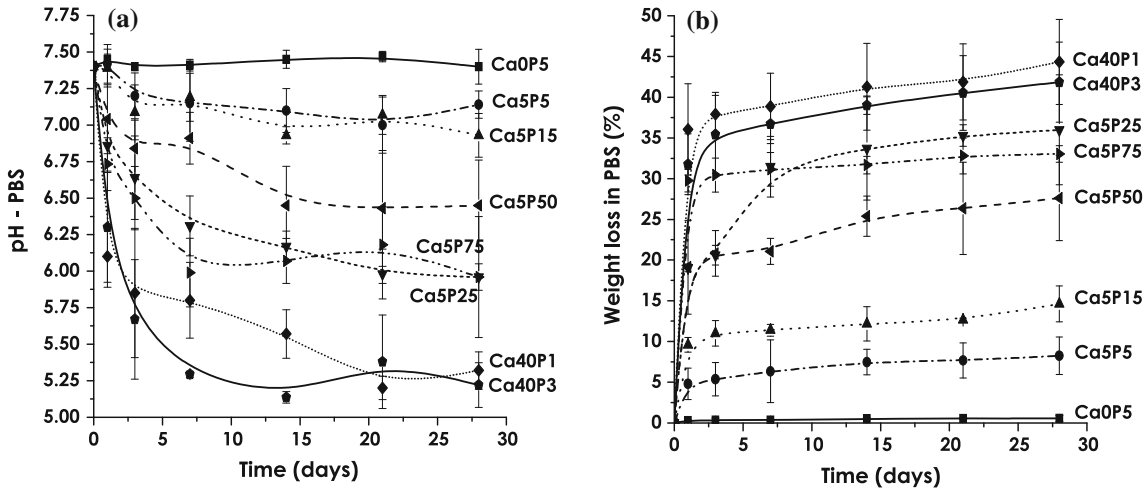

Fig. 8 **a** pH variation of hybrid materials soaked in PBS. **b** Weight loss of the hybrid material soaked in PBS

appearance of the materials. Densities lower than 1 g/cm^3 indicate that the materials tend to float when being immersed in a buffer solution. While the material Ca0P5 presents a great degree of hydrophobicity which can be attributed to PDMS that has a great effect on the material SiO_2 network, the material Ca5P75 completely sinks. When increasing the amount of phosphate groups, the materials' density also increases. On the other hand, whereas the amount of CaO increases, the materials' density decreases, due to their high porosity.

In vitro assays, degradability, bioactivity, and cytotoxicity

The stability or degradation of specimens of different compositions when soaked in PBS is described in Fig. 8. pH evolution is shown in Fig. 8a and weight losses in Fig. 8b. The initial pH is 7.4. When analyzing the variation of pH in PBS over the 28 days in Fig. 8a, a strong influence of the phosphate and calcium content on the materials can be observed. Also, a strong correlation between changes in pH buffer solution and the amount of weight loss in the materials can be appreciated. The higher the variation in pH, the greater the materials' weight loss; whereas the opposite is also observed for a small pH change, a small weight loss is appreciated [10, 30]. The hybrid material Ca0P5 exhibits a slight increase in pH above 7.4, with a minimal weight loss of only 0.6 ± 0.4 %. The material Ca5P5 has a decrease from 7.4 to 7.42 ± 0.13 pH during the first day of immersion, losing more than a half of its total weight, 4.80 ± 1.94 %; but in the 28th day, the buffer suffers a slight pH increase, reaching a final value of 7.14 ± 0.09 and the materials, a total weight loss of 8.25 ± 2.30 %. On the other hand, the material Ca5P15 has some pH fluctuations

during the 28 days of immersion. This material loses 14.62 ± 2.19 % of the total weight, and the buffer reaches a final pH value of 6.93 ± 0.14 during the 28 days. Ca5P25 induces a continuous decrease in the buffer pH, having a final value of 5.96 ± 0.41. Analyzing its behavior, this material loses in the first day of immersion more than a half of its total weight, a loss of 19.05 ± 0.48 %. On the 7th day, the material presents a sharp increase in weight loss, reaching a weight loss of 31.45 ± 3.72 %, and at the 28th day of immersion the material loses a maximum weight of 36 ± 6 %. The material Ca5P50 also shows a continuous decrease in pH, having a final value of 6.45 ± 0.31. As the materials described above, the material Ca5P50 loses more than a half of the total percentage of its weight during the first day, achieving a final weight loss of 27.61 ± 5.21 %. The material Ca5P75 presents a final pH value of 5.96 ± 0.09. After the first day of immersion, when the material losses great percentage of its total weight loss, it keeps a nearly constant weight, losing only 4 % of weight from the first day to the 28th day, reaching a final weight loss of 33 ± 1 %. Finally, the materials with the highest calcium content, Ca40P1 and Ca40P3, suffer a drastic decrease in pH and therefore a great weight loss since the first day of immersion, presenting the pH final values of 5.32 ± 0.12 and 5.22 ± 0.15, respectively. Then, they show a continuous weight loss, presenting losses of 44.33 ± 5.21 and 41.84 ± 4.91 %, respectively.

The results from FT-IR spectroscopy, XRD, and SEM show the degradation and crystallization of apatite on the surface of the Ca5P5, Ca5P15, Ca5P25, Ca5P50, Ca5P75, Ca40P1, and Ca40P3 hybrid materials since the first day of immersion in PBS. Figure 9 shows the FT-IR spectra and XRD patterns of the hybrid material Ca5P5 before and after being soaked in PBS. The FT-IR spectra in Fig. 9a show the disappearance of the bands at 743, 1339, and 1419 cm^{-1}. These bands associated to nitrate groups (NO_3^{1-}) disappear since the first day of immersion, indicating that those groups are washed into the buffer solution. The wide band attributed to Si–O–Si from SiO_2 network, PO_4 from phosphate structure (P_2O_5), and P–O/Si–O–Si bonds from the bridging units P–O–P and P–O–Si/[SiO_2] gets stronger, and the bands at 1070 and 1030 cm^{-1} are stronger in comparison with these same bands in the spectrum of the material before soaking in PBS, suggesting an increase in phosphate groups PO_4 due apatite crystallization [29]. The XRD patterns of the hybrid material Ca5P5 in Fig. 9b exhibit maxima at 21.7°, 25.8°, 31.7°, and 45.4°, after only 1 day of immersion. These maxima can be assigned to a crystalline apatitic phase [10, 28, 31]. The SEM photographs of the hybrid material Ca5P5 in Fig. 9c show a small degree of degradation, its particles are less interconnected, and the number and size of pores slightly increase.

The SEM pictures taken of Ca5P5, Ca5P15, Ca5P25, Ca5P50, Ca5P75, Ca40P1, and Ca40P3 show the appearance of a needle-flake structure on the surface after only 1 day of immersion. Then, the morphology of these structures evolves to plate, flake, flower, and dumbbell shapes, with variable sizes over time. Figure 10 shows SEM photographs of the hybrid material Ca5P5 before and after being soaked in PBS as an example.

The results of the cytotoxicity assay displayed in Fig. 11 show the viability of osteosarcoma on the materials Ca5P5, Ca5P15, Ca5P25, Ca5P50, Ca5P75, Ca40P1, and Ca40P3. The cellular viability is over 70 % at all times for each composition. These results show the non-cytotoxic effect of the materials for the osteosarcoma-like cells.

Discussion

Hybrid materials are known for their outstanding chemical and physical properties [32]. Changes in compositions play a pivotal role in hybrids' properties, not only because of the intrinsic properties they induce, but also because they affect the reaction kinetics and as a consequence the obtained structure. As it can be observed in Fig. 1 and according to the gelling times shown in Fig. 2, the hydrolysis–polycondensation reactions [33] occur simultaneously to form a continuous inorganic matrix. The structure and characteristics of the formed materials would depend on how those reactions evolve, affecting their structures and morphologies [34]. When the hydrolysis reactions occur faster, gelling times decrease, the volume of pores increases, and therefore the materials' density decreases (Table 1). The above could be understood as follows. Some of the Si–OH and P–OH groups get trapped by the large molecules formed at the beginning of the reactions, having no chance to react, consequently inducing the formation of porous gels with a less degree of polymerization, which may result in the decrease of their densities; but, when the hydrolysis–polycondensation reactions are slower, a greater degree of polymerization is allowed and more dense materials are formed. The formation of a three-dimensional SiO_2–P_2O_5 network in the materials can be observed clearly in Figs. 3a and 4, mainly in the band at 848 cm^{-1} assigned to (PDMS) Si–O–Si (TEOS) bonds and the band at 1100 cm^{-1} attributed to P–O bonds related to P–O–Si and P–O–P units in the FT-IR spectra and in the chemical shift of ~ -110 ppm corresponding to Q_3 and Q_4 structural units in the ^{29}Si MAS-NMR spectra, respectively. According to Almeida [14] and Neeraj [24], the chemical shifts in the MAS-NMR spectra displayed in Fig. 4 that make up structural Q units in the hybrid materials and phosphosilicates are located in -105 ppm (Q_3) and -111 ppm (Q_4), suggesting that

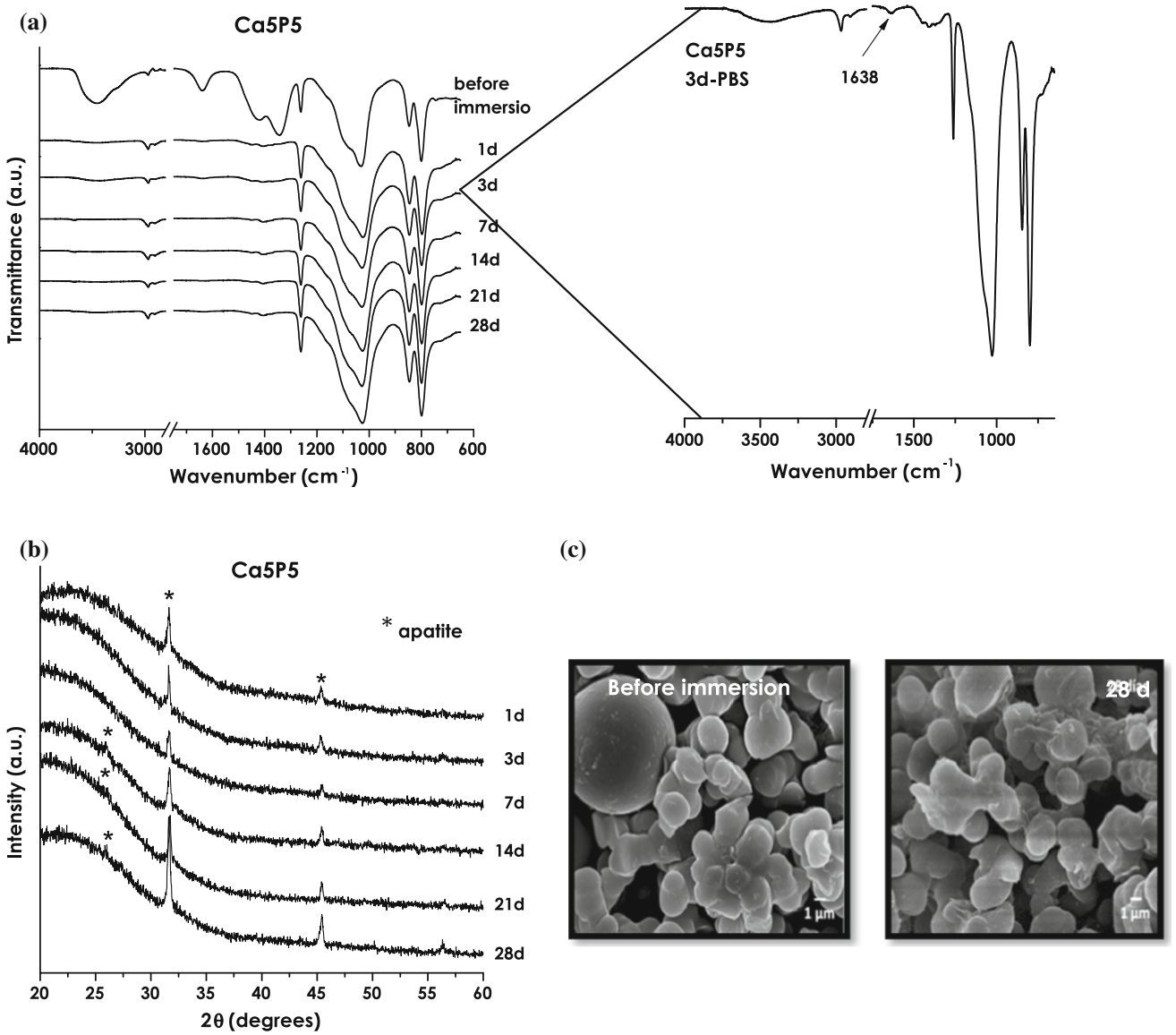

Fig. 9 **a** FT-IR spectra of the hybrid material Ca5P5 after different days of immersion in PBS. **b** XRD pattern of the hybrid material Ca5P5 after different days of immersion in PBS. **c** SEM photographs of the hybrid material Ca5P5 before and after immersion in PBS

Ca0P5 may exhibit a coordination number equal to four. Moreover, the amorphous structure of the hybrid materials and the influence of their composition on their structures can be appreciated deeply by studying the XRD patterns in Fig. 3b. Changes in the XRD patterns can be attributed to P_2O_5 and calcium content. P_2O_5 acts as a glass network former and contributes to the formation of the agglomerates of particles, which are considered to be responsible for the diffraction intensity. On the other hand, when analyzing the effect of calcium on the materials (Ca5P5, Ca40P1, and Ca40P3), it can be observed that the maximum at around 22.5° loses intensity and almost disappears in the materials with greater calcium content (Ca40P1 and Ca40P3). This happens because Ca divalent cations cause a discontinuity in the network by breaking bonds or inhibiting polycondensation reactions, causing a greater degree of internal disorder in the materials. On the other hand, the evolution from hybrid gels to glasses and then to glass-ceramics is shown in Figs. 5, 6, and 7. This evolution is produced when the materials are heated at lower and higher temperatures than the ones at which the materials transform into glasses and glass-ceramics. When the materials are thermally treated, the elimination of water, monomers, and ethanol occurs by diffusion. Condensation reactions still happen, helping decrease the number of pores and their sizes by the dehydration of silanol and phosphanol groups, producing a contraction within the materials' structure and an increase in their densities. The transformation evolution of a discontinuous structure of

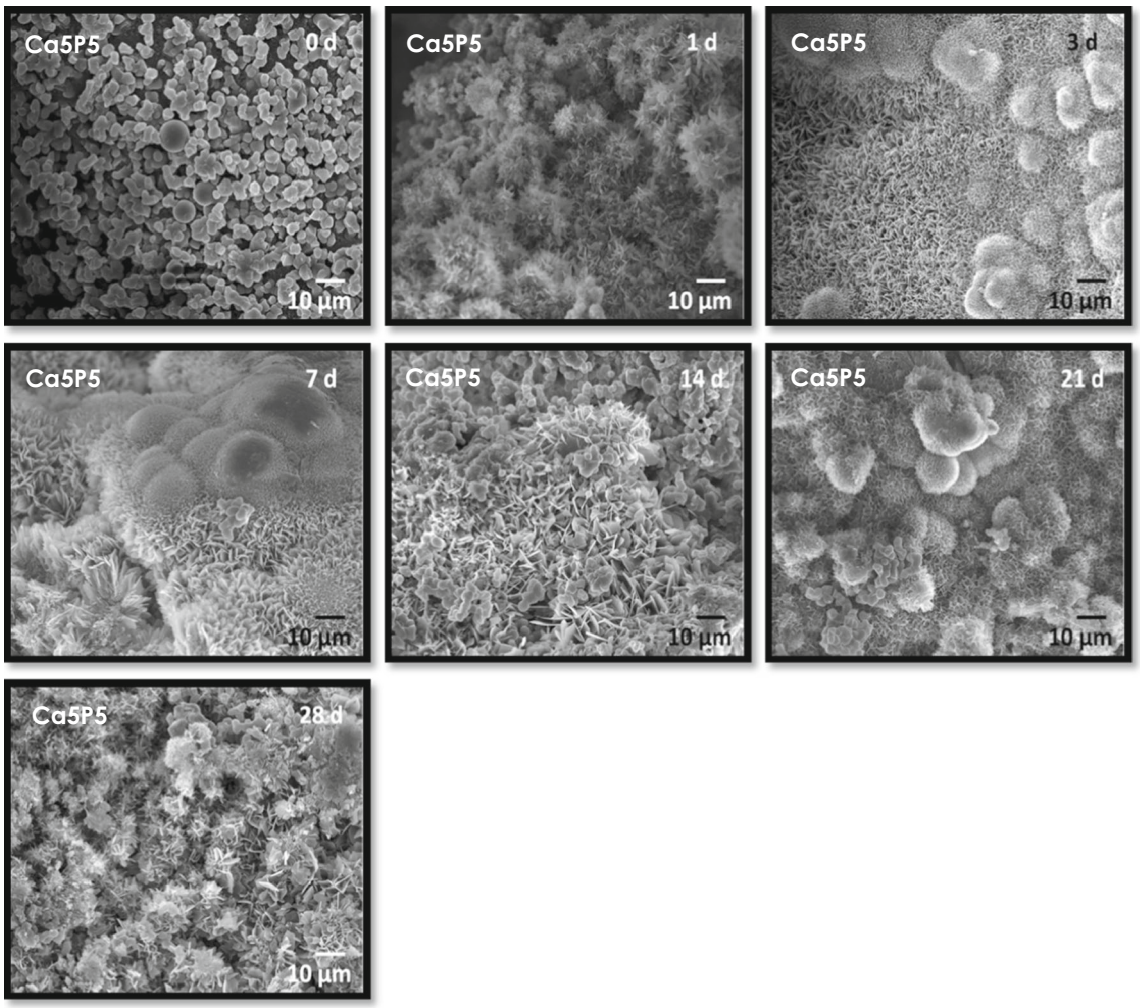

Fig. 10 SEM micrographs of the Ca5P5 hybrid material before and after immersion into PBS

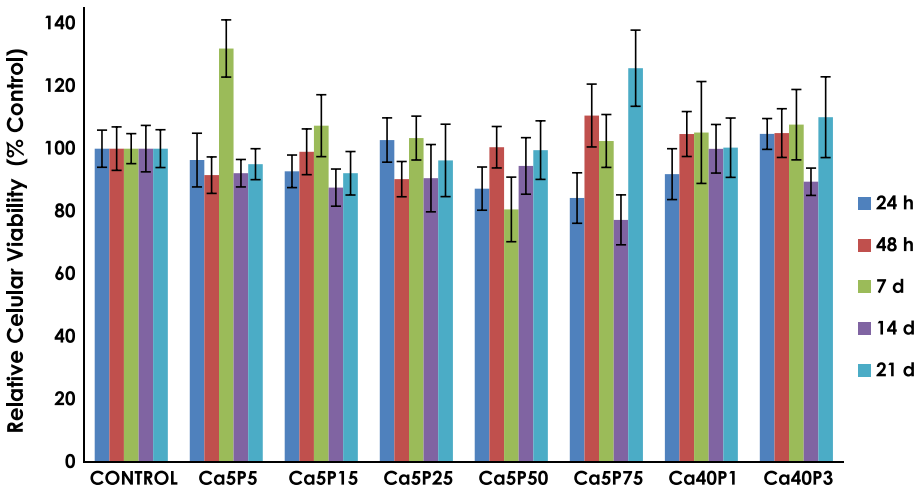

Fig. 11 Results of the cytotoxicity MTT assay at 1, 2, 7, 14, and 21 days

SiO_2 gels into a more typical continuous network of the glasses is seen in Fig. 7; this structural change of the materials occurs at about 700–800 °C, although the formed glasses will devitrify easily at lower temperatures in comparison to glasses manufactured at common methods, due to residual OH^- groups [22].

The pH changes and weight losses in the materials, shown in Fig. 8, help predict their hydrolytic degradation process. The organic degradation of PDMS in the hybrids is determined by several factors such as their structure, type of copolymerization, crystallinity, unreacted monomers, molecular weight, morphology, bond types, and porosity [35]. Furthermore, the degradation of the inorganic part in the materials is determined by a surface degradation mechanism, which is highly dependent on the pH of the surrounding medium, being more sensitive to acidic media. The minimum weight loss experienced by the Ca0P5 hybrid can be related to its highly hydrophobic behavior, observed when the material floated while being soaked in PBS. On the other hand, the material Ca5P75 was expected to have a continuous weight loss over time, due to the high solubility as a result of the hydrolysis of the large amount of phosphate groups within its network, through the breaking of the Si–O–P and P–O–P bonds. However, this is not observed and this is the only material that breaks into small pieces since the first day of immersion, which may promote faster solubility in further days. According to the above analysis, when increasing the amount of phosphate groups, the weight loss in the materials is more, due to the facility of phosphate groups to be hydrolyzed (P–OH). The materials with a greater amount of calcium, a network modifier, lose a greater amount of weight, thanks to their high porosity and hygroscopic behavior. Degradation in vitro studies [10, 36] have shown that highly porous materials begin to degrade faster than those with low porosity, since those materials exhibit a larger contact area in which the buffer solution can interact, facilitating the degradation of silanol groups from PDMS chains and SiO_2. On the other hand, materials with low contents of calcium and phosphate (Ca0P5, Ca5P5, and Ca5P15) show more cross-linked structures, since the SiO_2-based network gets little interrupted. This kind of highly interconnected SiO_2 network in the materials hinders the buffer solution interaction with their surfaces during the first day of immersion. The changes in the FT-IR spectra shown in Fig. 9a suggest that the degradation induces a frequency shift, an increase in bandwidth, and/or the appearance of new bands attributed to the degradation species [37]. In Fig. 9a, adsorption bands of Si–O–Si bonds related to [SiO_2], (TEOS) Si–O–Si (PDMS), and Si–CH_3 can be observed as described previously. No great changes can be identified in those spectra, and therefore the hybrid material does not have an important degradation neither in both of its portions, the organic and inorganic. It is worth to say that the weak band near ~ 1635 cm^{-1} appears since the first day of immersion, which is related to hydroxyl groups (OH–), which may suggest hydrolysis [37] of the material into Si–OH and P–OH groups and the crystallization of apatite [29]. This little degradation has an effect in the morphology, since the particles are less interconnected and the size and number of pores increase (Fig. 9c). According to different works in which bioactive materials are studied [17, 29, 38, 39], peaks attributed to apatite appear in the diffraction patterns of the material Ca5P5 in Fig. 9b. This material has a continuous apatite growth since the first day of immersion in PBS, indicating that calcium and phosphate promote apatite growth on the material surface. The hybrid materials have an organic–inorganic (PDMS–SiO_2) network characterized by a three-dimensional model of silica glass with linear PDMS chains which break the continuity of SiO_2 network by modifying their chemical properties and causing a decrease in their specific surface area, since the large –CH_3 molecules of PDMS get placed on the materials' surfaces hindering the materials' reactivity to PBS or SBF by inhibiting the presence of silanol groups, which are required for apatite formation during bioactive process [40]. According to the principles explained above, the degree of bioactivity in the studied materials is strongly linked to their nanostructure, since the distance between tetrahedral [SiO_4^{4-}] decreases when decreasing the calcium content within the materials' network. In the same way, when increasing phosphate content, tetrahedral SiO_2 bond to tetrahedral PO_4 forming silicone nuclei doped with calcium phosphate particles that promotes apatite precipitation on the materials' surfaces. The apatite growth with no preferential orientation and different crystal sizes during the 28 days of immersion in PBS is shown in Fig. 10. The variation in the morphology of crystallized apatite on the material surface can be related to the amount of calcium ions released when soaked in PBS and can be modified by the increase of phosphate groups and their degradation over time. The apatite morphologies that precipitate on the surface correspond to plate, flake, flower, and dumbbell shapes, with variable sizes over time. These shapes are related to the degree of saturation of calcium, phosphorous, and other ions and to the pH changes in PBS. Former studies have proved [41] that apatite chemically precipitated in solution is a very stable calcium phosphate phase and a less-soluble apatite type. Based on the results, it is suggested that the hydration of the Ca5P5 material leads to the formation of a gel made of silanol groups (Si–OH) on its surface and, together with the release of calcium and phosphorous ions coming from the chemical composition of the material in contact with more phosphorous ions and other dissolved salts in PBS, encourages and promotes the precipitation of apatite crystals. According to Kokubo [42], Padilla et al. [43], and Ohtsuki et al. [44], the nucleation and growth of the apatite layer on bioactive materials containing CaO–SiO_2 start by an exchange between Ca^{2+} ions in the materials and H_3O^+ groups in the solution, enhancing the formation of Si–OH groups on the surface and inducing the apatite nucleation. Since the growth of apatite depends on the ions in the solution and on the releasing of more Ca^{2+} ions from the material, larger contents of calcium decrease

the active surface of the materials. The calcium causes a larger number of smaller silicone–SiO_2 blocks, facilitating the dissolution and supersaturation of the solution with Ca^{2+} ions and promoting a continuous precipitation–dissolution cycle of apatite. Moreover, according to Mami et al. [45] and Mozafari et al. [28], the release of calcium ions into the solution is not only related to the calcium content in the materials' matrix, but also influenced by the textural parameters. Materials with a higher specific area show a greater release of calcium, and larger cylindrical pores help the calcium diffusion through the materials' matrix. The materials Ca5P5 and Ca5P15 meet the characteristics described above, enhancing their apatite crystallization and therefore their bioactivity behavior. The results arisen in the present study show that both Si–OH and Ca^{2+} seem to be more important than PO_4 in the improvement in the bioactive behavior of the materials, since Si–OH and Ca^{2+} favor a greater number of nucleation sites and a more orderly and homogeneous apatite growth. The opposite occurs when the phosphate groups increase, changing the structure of the materials by reducing the vitreous silica and therefore modifying their morphology, bioactive behavior, and orientation of apatite growth. The viability of the materials shown in Fig. 11 indicates that phosphate and calcium in adequate contents promotes cell viability and apatite crystallization, whereas high concentration of P_2O_5 may affect cell viability and high concentration of calcium may decrease pH values in buffer solution; but contrary to expectations this does not affect cell viability.

Conclusions

Hybrid materials based on the PDMS–P_2O_5–CaO–SiO_2 systems have been synthesized. Properties of the hybrids can be modified by designing the ratio of components of those hybrids. Materials with greater contents in CaO yield faster reaction kinetics and produce highly porous materials with large particle sizes up to 10 μm that favor a quicker degradation. Hybrids with greater P_2O_5 contents yield slower reaction kinetics and produce dense materials with particle sizes >100 nm and laminar structure of ~10 μm length that hinder the degradation kinetics. All tested materials, except Ca0P5, are bioactive, but Si–OH groups and Ca ions seem to be more important than PO_4 groups in the improvement in the bioactive behavior of the hybrids. All the compositions of the assayed systems are non-cytotoxic.

Acknowledgements This work was supported by DGICT Project, MAT2014-51918-C2-1-R, Spain, and SIP-IPN 20140064 Project, Mexico. DA Sánchez-Téllez also acknowledges CONACYT for the scholarship.

References

1. Sayed AA, Agarwal M, Giannoudis PV, Matthews SJE, Smith RM (2004) Distal femoral fractures: long term outcome following stabilization with the LISS. Injury 35:599–607
2. Zhao G, Zinger O, Schwartz Z, Wieland M, Landolt D, Boyan BD (2006) Osteoblast-like cells are sensitive to submicron-scale surface structure. Clin Oral Implant Res 17(3):258–264
3. Miyazaki T, Kamitakahar M, Ohtsuki C (2009) Chapter 16: development of bioactive organic-inorganic hybrids through sol-gel processing. In: Merheri L (ed) Hybrid nanocomposites for nanotechnology. Springer Science + Business Media, LLC, New York, pp 769–793
4. Yang Y, Kang Y, Sen M, Park S (2011) Chapter 7: bioceramics in tissue engineering. In: Burdick JA, Mauck RL (eds) Biomaterials for tissue engineering applications. Springer, Wien, pp 179–207
5. Rodríguez-Lorenzo LM (2014) Functionalized apatite nanocrystals for biomedical applications. In: Lafisco M, Delgado-López JM (eds) Apatite: synthesis, structural characterization and biomedical applications. NOVA Publishers, New York, pp 261–290
6. Dorozhkin SV (2009) Calcium orthophosphate-based biocomposites and hybrid biomaterials. J Mater Sci 44:2343–2387
7. Dorozhkin SV (2010) Bioceramics of calcium orthophosphates. Biomaterials 31:1465–1485
8. Hesaraki S, Alizadeh M, Nazarian H, Sharifi D (2010) Physicochemical and in vitro biological evaluation of strontium/calcium silicophosphate glass. J Mater Sci Mater Med 21:695–705
9. Lee KY, Lee YH, Kim HM, Koh MY, Ahn SH, Lee HK (2005) Synthetic model of a bioactive functionally graded nanohybrid in silica-polydimethylsiloxane system. Curr Appl Phys 5:453–457
10. Sánchez-Téllez DA, Téllez-Jurado L, Chávez-Alcalá JF (2014) Bioactivity and degradability of hybrids nano-composites materials with great application as bone tissue substitutes. J Alloys Compd 615(1):670–675
11. Brinker CJ, Scherer GW (1990) Sol-gel science: the physics and chemistry of sol-gel processing edit. Academic Press Inc. An Imprint of Elsevier, New York. ISBN.-13:978-0-12-134970-7
12. D'Apuzzo M, Aronne A, Esposito S, Pernice P (2000) Sol-gel synthesis of humidity-sensitive P_2O_5-SiO_2 amorphous films. J Sol-Gel Sci Tech 17:247–254
13. Ma J, Chen CZ, Wang DG, Meng XG, Shi JZ (2010) Influence of the sintering temperature on the structural feature and bioactivity of sol-gel derived SiO_2-CaO-P_2O_5 bioglass. Ceram Int 36:1911–1916
14. Almeida JC, Castro AGB, Lancastre JJH, Miranda Salvado IM, Margaca FMA, Fernandes MHV, Ferreira LM, Casimiro MH (2014) Structural characterization of PDMS-TEOS-CaO-TiO_2 hybrid materials obtained by sol-gel. Mater Chem Phys 143: 557–563
15. Téllez L, Rubio J, Rubio F, Morales E, Oteo JL (2004) FT-IR study of the hydrolysis and polymerization of tetraethyl orthosilicate and polydimethyl siloxane in the presence of tetrabutyl orthotitanate. Spectrosc Lett 37:11–31
16. Salinas AJ, Merino JM, Babonneau F, Gil FJ, Vallet-Regí M (2007) Microstructure and macroscopic properties of bioactive CaO-SiO_2-PDMS hybrids. J Biomed Mater Res B 81B:274–282
17. Whang C, Seo D, Oh E, Kim Y (2005) Compositional dependence of apatite formation in sol-gel derived organic-inorganic hybrids. Glass Phys Chem 31(3):396–401
18. Vallet-Regí M, Salinas AJ, Ramírez-Castellanos J, González-Calbet JM (2005) Nanostructure of bioactive sol-gel glasses and organic-inorganic hybrids. Chem Mater 17:1874–1879

19. Sava BA, Elisa M, Vasiliu LC, Nastase F, Simon S (2012) Investigation on sol-gel process and structural characterization of SiO_2-P_2O_5 powders. J Non-Cryst Solids 358:2877–2885
20. Padilla S, Román J, Carenas A, Vallet-Regí M (2005) The influence of the phosphorus content on the bioactivity of sol-gel glass ceramics. Biomaterials 26:475–483
21. Massiot Ph, Centeno MA, Carrizosa I, Odriozola JA (2001) Thermal evolution of sol-gel-obtained phosphosilicate solids (SiPO). J Non-Cryst Solids 292:158–166
22. Fernández-Navarro JM (1991) El vidrio. Edit. Consejo Superior de Investigaciones Científicas. Fundación Centro Nacional del Vidrio. 2nd edn, Spain. ISBN: 84-00-07130-1
23. Glaser RH, Wilkes GL, Bronnimann CE (1989) Solid state ^{29}Si NMR of TEOS-based multifunctional sol-gel materials. J Non-Cryst Solids 113:73–87
24. Neeraj Eswaramoorthy M, Rao CNR (1998) Mesoporous silicophosphate. Mater Res Bull. 33(10):1549–1554
25. Carta D, Newport RJ, Knowles JC, Smith ME, Guerry P (2011) Sol-gel produced sodium calcium phosphosilicates for bioactive applications: synthesis and structural characterization. Mater Chem Phys 130:690–696
26. Brow RK (2000) Review: the structure of simple phosphate glasses. J Non-Cryst Solids 263&264:1–28
27. Siqueira RL, Zanotto ED (2011) Facile route to obtain a highly bioactive SiO_2-CaO-Na_2O-P_2O_5 crystalline powder. Mater Sci Eng C 31:1791–1799
28. Saboori A, Rabiee M, Moztarzadeh F, Sheikhi M, Tahriri M, Karim M (2009) Synthesis, characterization and in vitro bioactivity of sol-gel-derived SiO_2-CaO-P_2O_5-MgO bioglass. Mater Sci Eng C 29:335–340
29. Mozafari M, Moztarzadeh F, Tahriri M (2010) Investigation of the physico-chemical reactivity of a mesoporous bioactive SiO_2-CaO-P_2O_5 glass in simulated body fluid. J Non-Cryst Solids 356:1470–1478
30. Tatai L, Moore TG, Adhikari R, Malherbe F, Jayasekara R, Griffiths I, Gunatillake PA (2007) Thermoplastic biodegradable polyurethanes: the effect of chain extender structure on properties and in vitro degradation. Biomaterials 28:5407–5417
31. John A, Mani S, Gopalakrishnam S, Babu S, Lal AV, Varma H (2011) Osteogenesis of a bioactive ceramic-calcium phosphosilicate composite system in goat femur defect. Int J Appl Ceram Technol 8(3):491–500
32. Jiménez-Gallegos R, Téllez-Jurado L, Rodríguez-Lorenzo LM, San Román J (2011) Modulation of the hydrophilic character and influence on the biocompatibility of polyurethane-siloxane based hybrids. Bol Soc Esp Ceram Vidr 50(1):1–8
33. Huang K, Cai S, Xu G, Ye X, Dou Y, Ren M, Wang X (2013) Preparation and characterization of mesoporous 45S5 bioactive glass-ceramic coatings on magnesium allow for corrosion protection. J Alloys Compd 580:290–297
34. Kim IY, Kawachi G, Kikuta K, Cho SB, Kamitakahara M, Ohtsuki C (2008) Preparation of bioactive spherical particles in the CaO-SiO_2 system through sol-gel processing under coexistence of poly(ethylene glycol). J Eur Ceram Soc 28:1595–1602
35. Gunatillake PA, Adhikari R (2003) Biodegradable synthetic polymers for tissue engineering. Eur Cells Mater 5:1–16
36. Guana J, Fujimotoa KL, Sacksa MS, Wagnera WR (2005) Preparation and characterization of highly porous, biodegradable polyurethane scaffolds for soft tissue applications. Biomaterials 26:3961–3971
37. Sabino M, Núñez O, Müller J (2002) Evidencias Espectroscópicas de la Degradación Hidrolítica de la Poli(dioxanona). Rev Latinoam de Metal y Mater 22(2):40–51
38. Miyata N, Fuke K, Chen Q, Kawashita M, Kokubo T, Nakamura T (2004) Apatite-forming ability and mechanical properties of PTMO modified CaO–SiO_2–TiO_2 hybrids derived from sol-gel processing. Biomaterials 25:1–7
39. Chikara O, Miyazaki T, Tanihara M (2002) Development of bioactive organic-inorganic hybrid for bone substitutes. Mater Sci Eng C 22:27–34
40. Sastre R, de Aza S, San Román J (2001) Biomateriales. Edit. CYTED Programa Iberoamericano de Ciencia y Tecnología para el Desarrollo, Italy. ISBN: 84-87683-26-6
41. Sadat-Shojai M, Khorasani M-T, Dinpanah-Khoshdargi E, Jamshidi A (2013) Review: synthesis methods for nanosized hydroxyapatite with diverse structures. Acta Biomater 9:7591–7621
42. Kim H-M, Himeno T, Kokubo T, Nakamura T (2005) Process and kinetics of bonelike apatite formation on sintered hydroxyapatite in a simulated body fluid. Biomaterials 26(21):4366–4373
43. Ragel CV, Vallet-Regí M, Rodríguez-Lorenzo LM (2002) Preparation and in vitro bioactivity of hydroxyapatite/sol gel-glass biphasic material. Biomaterials 23(8):1865–1872
44. Ohtsuki C, Miyazaki T, Kamitakahara M, Tinihara M (2007) Design of novel bioactive materials through organic modification of calcium silicate. J Eur Ceram Soc 27:1527–1533
45. Mami M, Lucas-Girot A, Oudadesse H, Dorbez-Sridi R, Mezahi F, Dietrich E (2008) Investigation of the surface reactivity of a sol gel derived glass in the ternary system SiO_2-CaO-P_2O_5. Appl Surf Sci 254:7386–7393